Extended Data Fig. 3 | Expression of the H-latch mimic R207C-I138C in organotypic cultured slices leads to dose-dependent neurotoxicity. (a) Flow cytometry gating strategy of PI positive CAD5 cells. **(b)** PNGase-F digestion of cell lysates induced a shift in both murine wild-type PrP^{C} and $mPrP^{2cys}$, indicating that both moieties had undergone N-linked glycosylation to a similar extent. Non-adjacent lanes were merged from the same gel. **(c)** CAD5 *Prnp*$^{-/-}$ cells expressing $mPrP^{2cys}$ did not show an upregulation of the unfolded protein response, suggesting that $mPrP^{2cys}$ did not undergo pathological degradation. Values are given as percentage of empty control vector (p-eIF2α / eIF2α / actin). One datapoint per group corresponds to a different cell culture passage. Two-sided, unpaired t-test. **(d)** A POM2/POM3 sandwich ELISA of COCS transduced with empty control, $mPrP^{C}$, $mPrP^{2cys}$ and buffer control shows robust $mPrP^{2cys}$ expression in transduced COCS, albeit significantly less than wild-type $mPrP^{C}$. Slices were harvested at 28 days post-transduction. One datapoint corresponds to an independent, biological replicate of 6–9 pooled slices. Ordinary, one-way Anova with Šídák's multiple comparisons test, *: adjusted p-value = 0.039 **(e)** Reduced levels of mNG in *Prnp*$^{-/-}$ (ZH3) COCS expressing $mPrP^{2cys}$. mNG immunoreactivity values are divided by actin immunoreactivity and expressed as percentages of empty control. Slices were harvested at 28 days post-transduction. One datapoint corresponds to an independent, biological replicate of 6–9 pooled slices. Ordinary, one-way Anova with Šídák's multiple comparisons test. Raw, uncropped blots can be found in the Source Data supplement. **(f)** Quantification of mNG and Calb1 fluorescence intensity from experiments shown in Fig. 3d-f. One datapoint corresponds to a biological replicate, e.g. one organotypic cultured slice. Unpaired, two-tailed t-test without adjustment for multiple testing. P-values are as follows: 31 dpt, $5.2x10^{10}$ vg*ml^{-1}, mNG: 0.001; 31 dpt, $5.2x10^{10}$ vg*ml^{-1}, Calb1: 0.0496; 15 dpt, $1.4x10^{11}$ vg*ml^{-1}, mNG: 0.0065; 15 dpt, $1.4x10^{11}$ vg*ml^{-1}, Calb1: 0.001. ***: $p \leq 0.001$, **: $p < 0.01$, * $p < 0.05$.

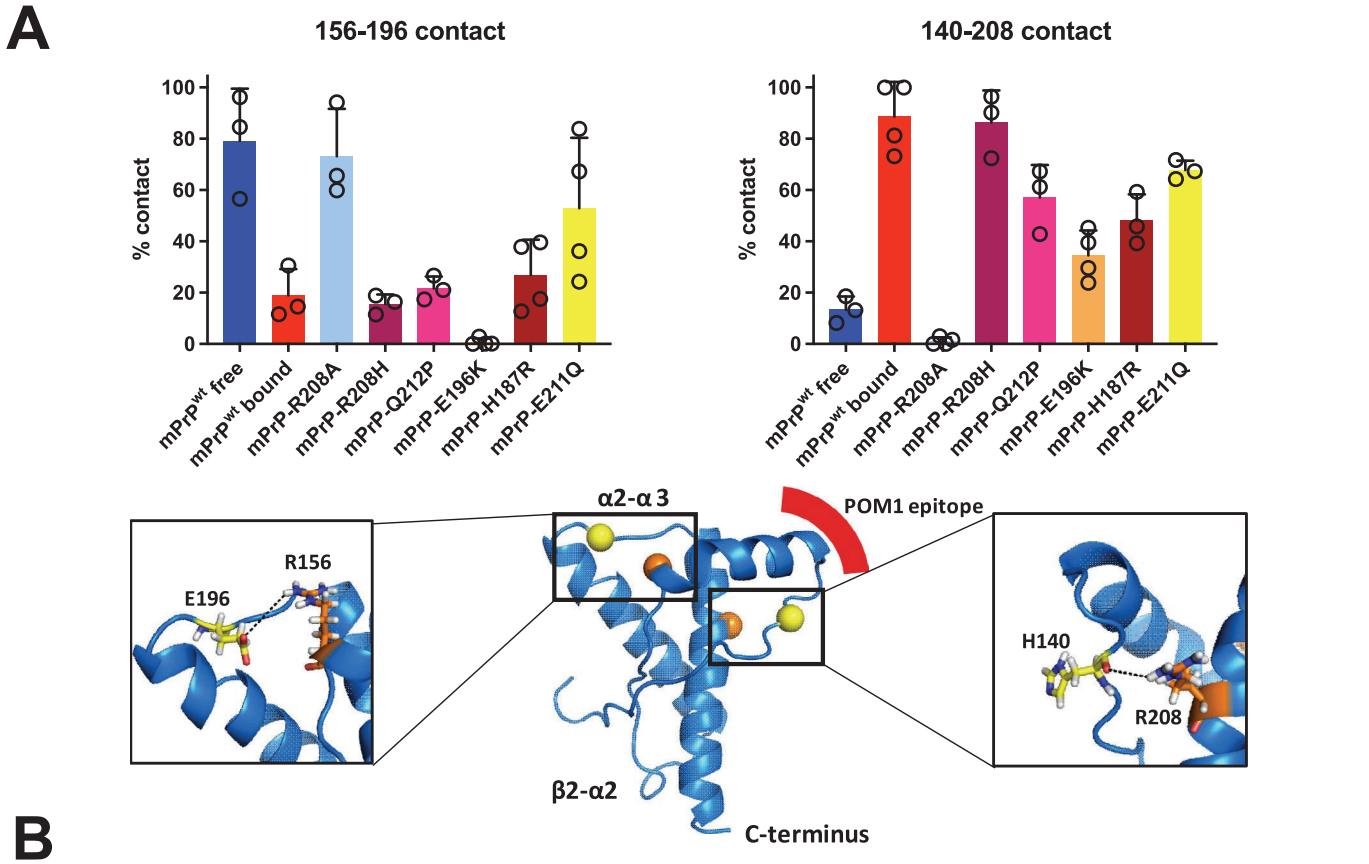

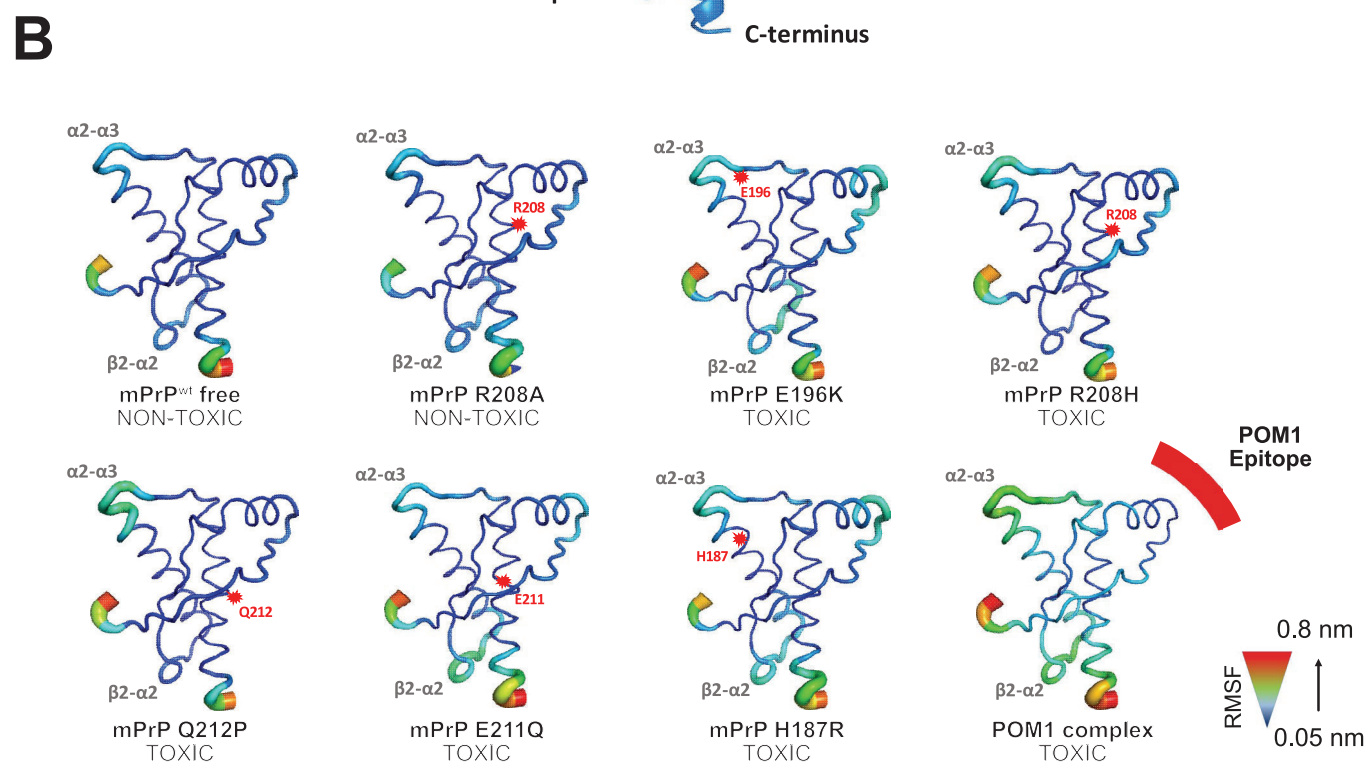

Extended Data Fig. 4 | Molecular dynamics simulations show overlapping structural changes of POM1-PrP^C complex and pathogenic *PRNP* mutations. Extended Data Figure 4. **(a)** MD simulations of POM1 binding and pathogenic *PRNP* mutations causing genetic prion disease show the R156-E196 interaction is abolished and induction of the H140-R208 H-latch is established. Each datapoint represents one independent simulation, values are given as mean ± standard deviation. **(b)** In agreement with this view, POM1 and human, hereditary PrP mutations responsible for fatal prion diseases favor altered flexibility in the α2-α3 and β2-α2 loop.

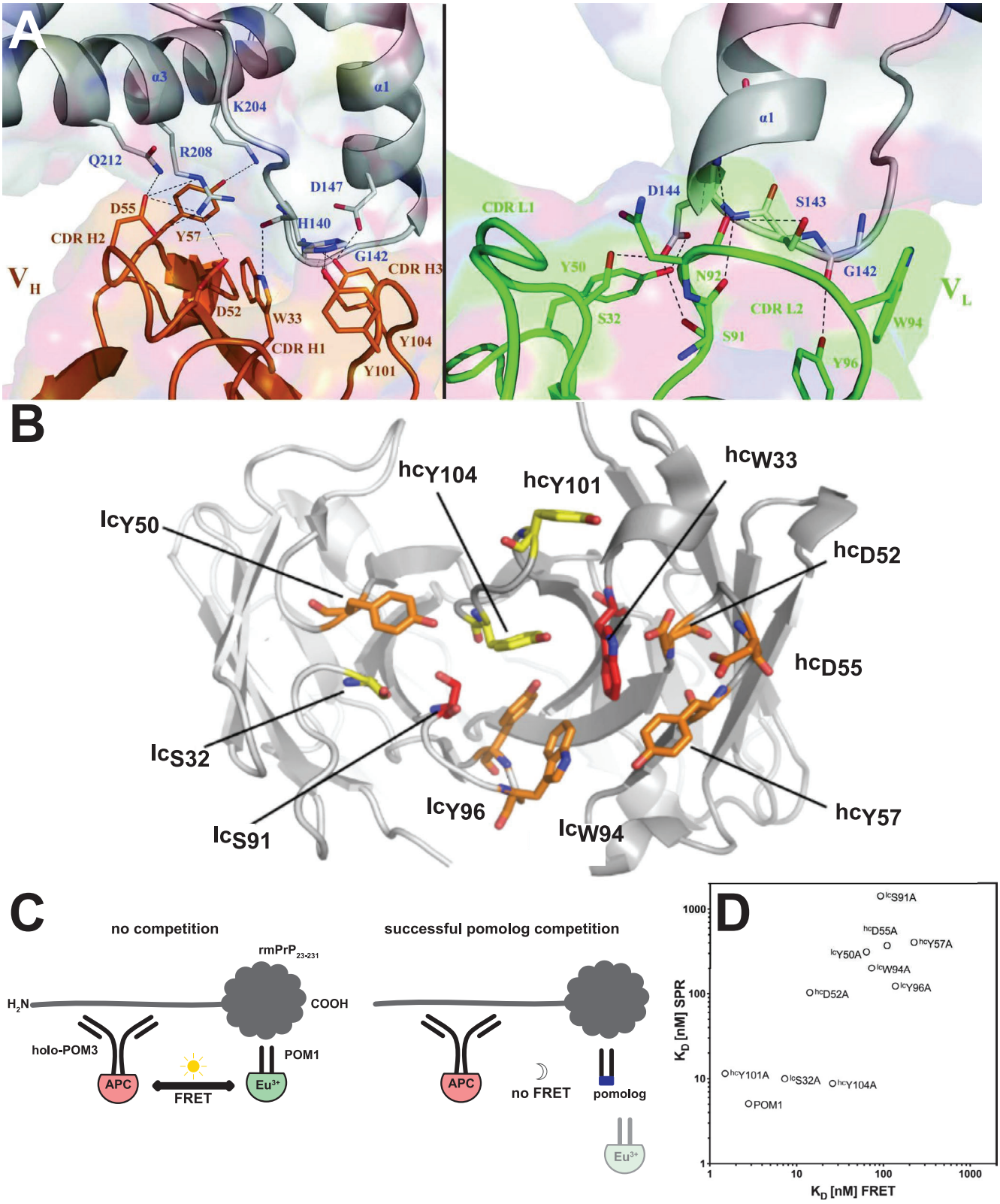

Extended Data Fig. 5 | See next page for caption.

Extended Data Fig. 5 | Scanning alanine mutagenesis of the POM1 paratope. Extended Data Figure 5. **(a)** Intermolecular contacts between human $PrP^{C}_{120-230}$ and POM1 Fab variable heavy chain (magenta, *left panel*), and POM1 Fab variable light chain (green, *right panel*) as determined by Baral et al., 2012[8]. Reproduced with permission of the International Union of Crystallography from doi:10.1107/S0907444912037328. **(b)** Schematic representation of a single-chain fragment of wild-type POM. The mutated residues are indicated as stick on the cartoon structure of POM1, color coded as in Supplementary Table 1b. The CDR loops are shown from the perspective of the antigen. **(c)** Scheme of competition FRET assay to assess the K_D of various pomologs. In the absence of competing antibody, FRET occurs due to proximity of allophycocyanin (APC)-labeled holo-POM3 and europium (Eu3+)-labeled POM1 (*left panel*). Because of liquid-phase competition, addition of unlabeled pomologs leads to a decrease in FRET signal (*right panel*). The calculation of binding constants from FRET is detailed in the methods section. **(d)** The binding constants measured by SPR and by FRET were in good agreement, Spearman $r = 0.77$, $p=0.0074$, 95% CI 0.30–0.94) with the exception of ^{hc}W33A, whose binding on SPR was too weak to be precisely measured.

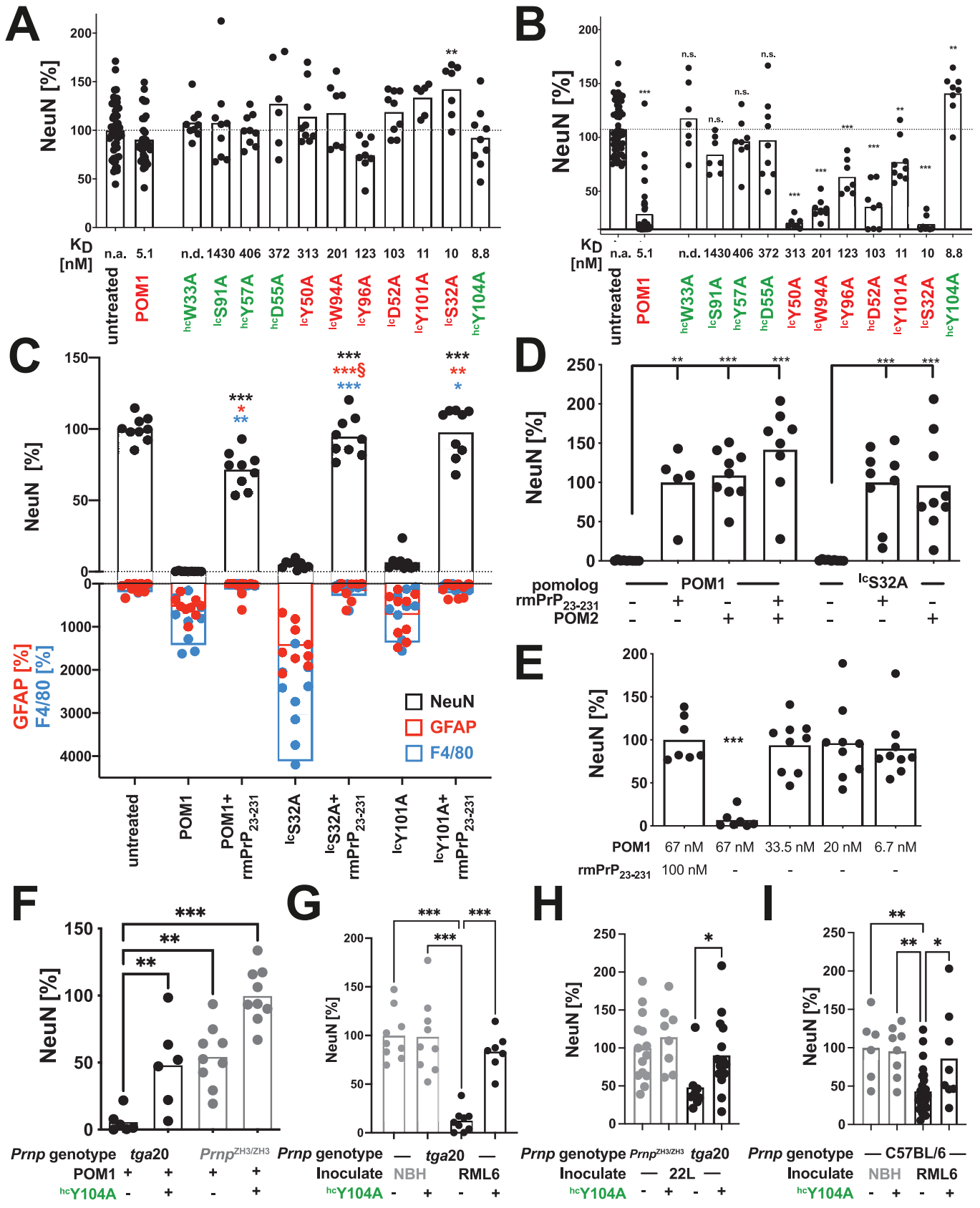

Extended Data Fig. 6 | See next page for caption.

Extended Data Fig. 6 | Pomolog ^{hc}Y104A acts as dominant negative suppressor of prion toxicity. Extended Data Figure 6. **(a)** Treatment of *Prnp*$^{ZH1/ZH1}$ COCS shows toxicity of POM1 and toxic pomologs to be dependent on PrP^{C}, see also Supplementary Fig. 1a. **: p=0.003, ordinary one-way Anova with Dunnett's multiple comparisons test. Innocuous pomologs are highlighted in green, POM1 and toxic pomologs are highlighted in red. **(b)** Morphometric quantification of *Prnp*-overexpressing tga20 COCS treated with pomologs, see also Fig. 4. Color coding according to panel (A). 100%=untreated COCS, comparison of untreated versus treated groups. N.s.: not significant, ***: $p < 0.0001$, ** ^{hc}Y101A: p=0.0035, ** ^{hc}Y104A: p=0.0019, ordinary one-way Anova with Dunnett's multiple comparisons test. **(c)** Morphometric quantification of fluorescence intensity from images depicted in Supplementary Fig. 1b. §: 1 outlier was excluded (y=2046.3%, $p < 0.05$, extreme studentized deviate method). Values = % of untreated control. Pairwise comparison in the presence or absence of rmPrP$_{23-231}$. ***: $p < 0.0001$, * GFAP-POM1: p=0.0148, ** GFAP-^{lc}Y101A: p=0.0009, ** F4/80-POM1: p=0.0005, * F4/80-^{lc}Y101A: p=0.0261, ordinary one-way Anova with Šídák's multiple comparisons test. **(d)** Toxicity of high-affinity pomolog ^{lc}S32A ablated by POM2. 100%=POM1 + rmPrP$_{23-231}$ (*bars 1–4*) or 100%=^{lc}S32 + rmPrP$_{23-231}$ (*bars 5–7*). ** p=0.0003, *** $p < 0.0001$, ordinary one-way Anova with Šídák's multiple comparisons test. **(e)** Titration of minimal toxic dosage of POM1 in tga20 COCS. 100%=POM1 + rmPrP$_{23-231}$. ***: $p < 0.0001$, ordinary one-way Anova with Dunnett's multiple comparisons test. **(f)** ^{hc}Y104A prevented POM1-induced toxicity. 100%=*Prnp*$^{0/0}$ COCS treated with POM1 + ^{hc}Y104A. ** p=0.0078, ***(left): p=0.0009, ***(right): $p < 0.0001$, ordinary one-way Anova with Dunnett's multiple comparisons test. **(g)** Quantification of Fig. 4b. 100%=untreated+NBH. ***: $p < 0.0001$, ordinary one-way Anova with Dunnett's multiple comparisons test. **(h)** Quantification of Fig. 4c. 100% = *Prnp*$^{ZH3/ZH3}$ + 22 L. *: p=0.032, ordinary one-way Anova with Šídák's multiple comparisons test. **(i)** Quantification of Fig. 4d. 100%=untreated +NBH. *: p=0.0203, **(left): p=0.0036, **(right): p=0.005, ordinary one-way Anova with Dunnett's multiple comparisons test. All graphs: one datapoint corresponds to one biological replicate.

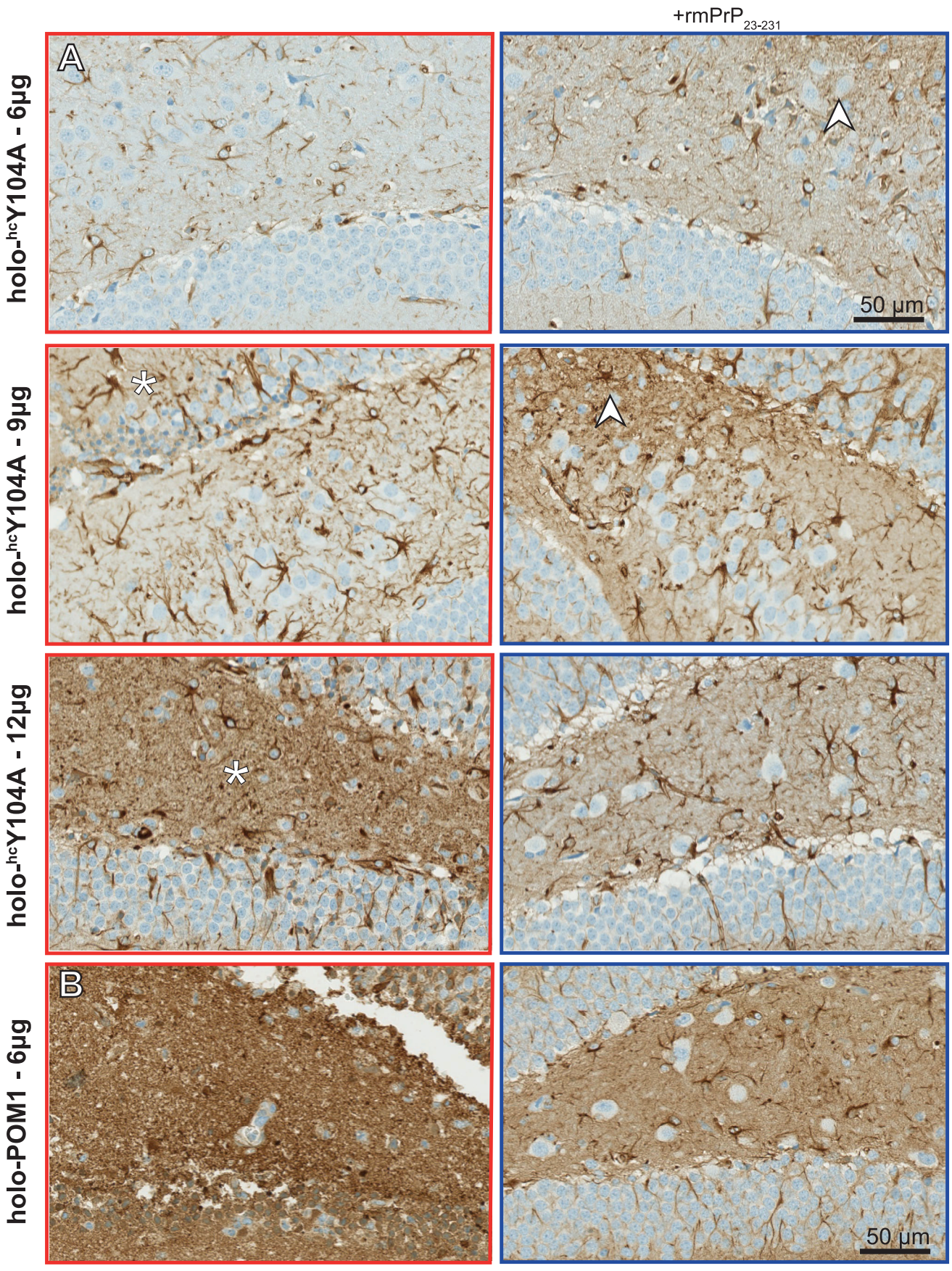

Extended Data Fig. 7 | See next page for caption.

Extended Data Fig. 7 | Dose-dependent gliosis of ^{hc}Y104A is also conspicuous around needle tracts. Extended Data Figure 7. (**a**) Photomicrographs of glial fibrillary acid protein (GFAP) immunohistochemistry on consecutive sections depicted in Fig. 6c. *Left column*: holo-^{hc}Y104A injections (6, 9 and 12 μg). *Right column*: holo-^{hc}Y104A + rmPrP$_{23-231}$. GFAP immunoreaction was increased in areas of neuronal damage (*white asterisks*) and around needle tracts (*white arrowheads*). (**b**) Micrographs demonstrating an intensive GFAP immunoreaction in areas with extensive holo-POM1 (6 μg)- induced neurotoxicity. *Left panel*: POM1 injection (6 μg). *Right panel*: holo-^{hc}Y104A + rmPrP$_{23-231}$. Sections are consecutive to those shown in Fig. 6f.

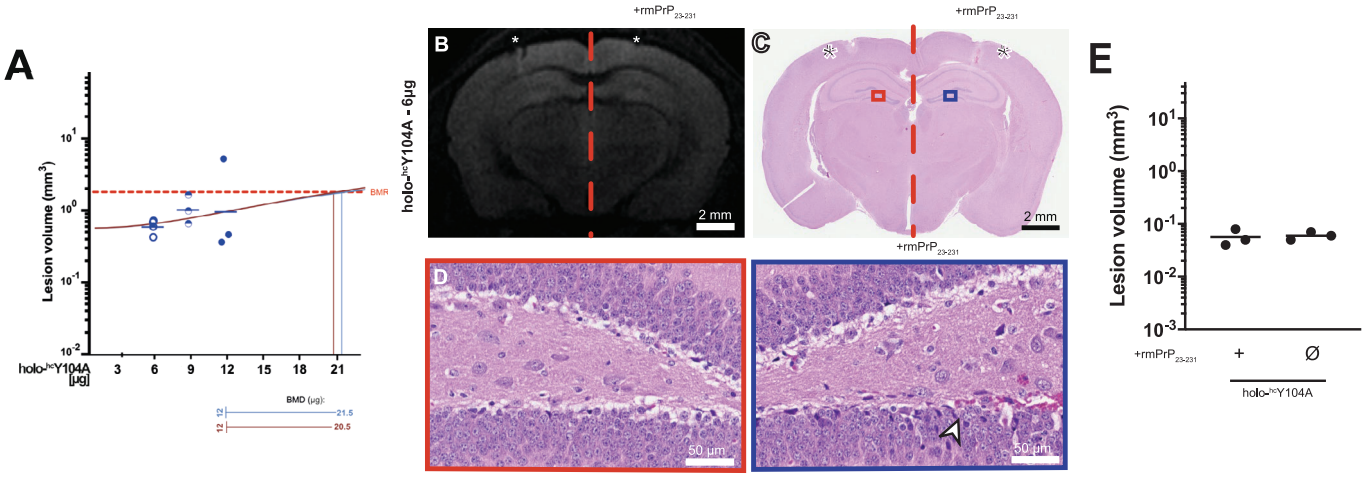

Extended Data Fig. 8 | Assessing ^{hc}Y104A dose-dependent toxicity. Extended Data Figure 8. **(a)** A hypothetical benchmark dose analysis was performed using log_{10}-transformed lesion volumes corresponding to different amounts of holo-^{hc}Y104A (data from Fig. 6g). BMR: Benchmark response (0.15 mm^3, dashed red line). The benchmark dose (BMD) is defined as the dose at the BMR. The vertical lines indicate the BMD values corresponding to the different dose response values (blue: 21.5 µg, brown line: 20.5 µg). The upper limit of the safe dose is provided by the lower 95% confidence interval of the BMD (horizontal lines below the graph: blue: 12 µg, brown: 12 µg). One datapoint corresponds to one independent animal. **(b)** Representative DWI images taken 24 h after stereotactic injection of 6 µg holo-^{hc}Y104A into male tga20 mice (*left half of the image*, injected into CA3). Contralateral side: 6 µg holo-^{hc}Y104A pre-incubated with an equimolar amount of $rmPrP_{23-230}$. *White asterisks*: needle tract. **(c)** Photomicrograph of HE-stained sections from mouse brain shown in panel B. *Asterisks*: needle tract. Rectangles correspond to regions magnified in panel C. **(d)** Higher magnification of the end-plate of the hippocampus. *Left panel*: holo-^{hc}Y104A. *Right panel*: holo-^{hc}Y104A preincubated with $rmPrP_{23-230}$. *Arrow*: needle tract. **(e)** Quantification of lesion volumes after injection of holo-^{hc}Y104A in contrast to control injection into tga20 mice (N = 3). One datapoint corresponds to one independent animal.